Numerical Simulation of Particle Deposition in Cross-Flow Microfiltration of Binary Particles

Kuo-Jen Hwang and Yun-Sheng Wang

Department of Chemical Engineering
Tamkang University
Tamsui, Taipei, Taiwan 251, R.O.C.

Abstract

The migration and the deposition of binary submicron particles in cross-flow microfiltration are simulated in this study. The forces exerted on particles are analyzed, and the Newton's second law of motion is integrated to simulate the velocities and displacements of particles near the membrane surface. The effects of operating conditions on the packing structure of particles and cake porosity are discussed. It can be found that the packing porosity of binary particles is smaller than those of mono-sized due to the cavern and the displacement effects. The simulated results show that looser packing for a given mixing fraction is constructed under a larger cross-flow velocity or a smaller filtration rate. The impact of the mixing fraction of binary particles is demonstrated by the experimental data of particle packing under gravity.

Key Words: Cross-Flow Microfiltration, Submicron Particles, Particle Deposition, Brownian Dynamic Simulation, Particle Packing

1. Introduction

Cross-flow microfiltration is increasingly used in many industries for purification or separation of submicron particles from liquids. Since the performance of microfiltration is affected by several major factors, such as the Brownian motion of particles, electrostatic interaction between particles, and hydrodynamics etc., this complex course has not been well understood yet.

When the diameter of particles ranged from 0.1 to 1.0 micrometers, the resistance of the filter cake plays the major role in the performance of a cross-flow filtration. Since the cake resistance is mainly determined by the amount and the structure of the formed cake, to understand how the particles migrate and deposit on the membrane surface are the essential steps in grasping the problem of such filtration.

Altena and Belfort [1] have used the hydrodynamic model to analyze the velocity distribution of fluid and the trajectories of particles in a cross-flow filtration system. The concentration profile and the transport flux of particles can be calculated accordingly. On the other hand, the selective deposition of particles in cross-flow filtration has been discussed [5, 9]. The external forces exerted on the particles staying on the membrane surface determine whether or not the particle can deposit stably. Lu and Hwang [10] have calculated the critical angle of friction between particles in a cross-flow filtration using a force balance model. The probability of particle deposition and the packing structure on the cake surface have been also simulated.

The Brownian dynamic simulation method has been widely used to simulate the migration of colloids in a flowing system. The particle trajectories can be traced by integrating Newton's second law of motion. The effects of colloidal and hydrodynamic interactions between particles on a sediment structure have been discussed by this method [2]. A more compact structure of sediment was constructed if the Brownian motion of

particles was taken into consideration. Ansell and Dickinson [3, 4] have extended the method of Brownian dynamic simulation to study the kinetics of colloidal coagulation in a simple shear flow. Lu *et al.* [11] have simulated the structures of filter cake formed in constant pressure cake filtrations by using the Brownian dynamic simulation method. The most compact cake was formed when the frictional drag and Brownian force are of the same order of magnitude. In recent years, Hwang et al. [7] have simulated the particle migration and deposition in cross-flow microfiltration of mono-sized submicron particles. The instantaneous cake formation, the probability of particle deposition and the packing structure under various operating conditions could be obtained.

In this article, a numerical program based on the Brownian dynamic simulation is established to trace the migration of binary submicron particles near the membrane surface in cross-flow microfiltration. The porosities of the packed structure at the initial stage of filtration under various operating conditions are estimated accordingly.

2. Analysis

2.1 Particle Trajectories

Fig.1 shows the cross-flow microfiltration system and defines the coordinates used in this analysis. The filter is constructed with two parallel plates, one of which is permeable. The filter channel has a height of *H*, a length of *L*, and a width of *W*. The velocity distribution in the cross-flow direction is parabolic, while the permeating is uniform if the filter is not very long. When particles are fed into the filter, some of them are carried by liquid toward the membrane surface and have opportunities to deposit stably. The filtration resistance is dependent on the mass and the packing structure of the formed cake. Therefore, to understand the particles how to migrate in the filter and how to deposit are very important in this course. In this study, the migration of particles near the cake surface is simulated in order to know the effects of operating conditions and particle size distribution on the cake porosity.

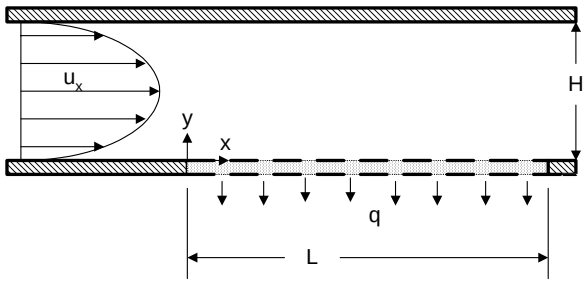

Figure 1. A schematic diagram of cross-flow microfiltration system.

Fig.2 depicts the major forces exerted on a depositing particle. The forces include the frictional drag force, F_d, the net gravity, F_g, the inertial lift force, F_l, the net interparticle force, F_i, and the Brownian force, F_B. For an incompressible spherical particle, the Newton's second law of motion can be written as

$$m_p \frac{dv_p}{dt} = F_d + F_g + F_l + F_i + F_B \qquad (1)$$

where m_p is the mass of the particle, v_p is the velocity of the particle, and *t* is time. Each term in the above equation should be analyzed prior to obtaining the instantaneous velocity or the displacement of the particle within a time increment.

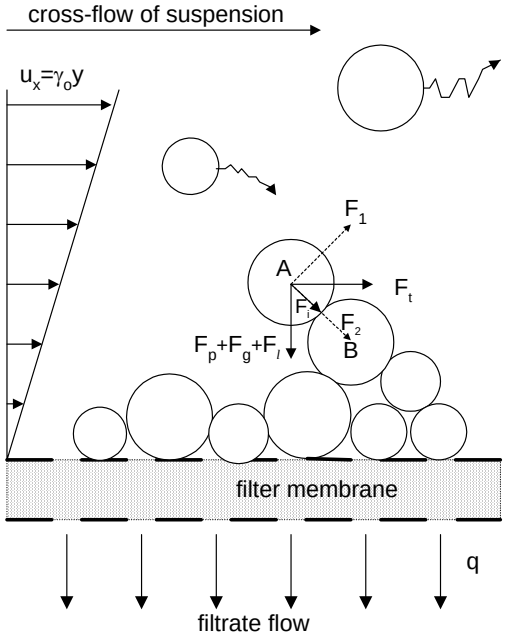

Figure 2. Forces exerted on a depositing particle in a cross-flow microfiltration.

1. Drag force due to fluid flow, F_d

The drag force exerted on the particle is determined by the local flow field of fluid and can

be divided into two components whose directions are either parallel or vertical to the cross-flow of suspension. They are analyzed below.

(1) F_{dx}

Since the velocity of tangential flow is very small near the membrane surface, the modified Stokes law can be employed to estimate the drag exerted on the particle in the x-direction, that is

$$F_{dx} = \frac{3}{4}\pi\mu\, d_p{}^2 \gamma_o C_x \qquad (2)$$

in which μ is the viscosity of liquid, d_p is the diameter of particle, γ_o is the shear rate at the membrane surface, and C_x is the correction factor of shear flow across a plane wall. According to the results of O'Neill [12], the correction factor is equal to 1.7009. The velocity distribution in the filter channel can be expressed as [7]:

$$u_x = 6u_s\left[\left(\frac{y}{H}\right)-\left(\frac{y}{H}\right)^2\right] \qquad (3)$$

where u_s is the average cross-flow velocity. Therefore, the shear rate at the membrane surface can be given by

$$\gamma_o = \left.\frac{du_x}{dy}\right|_{y=0} = \frac{6u_s}{H} \qquad (4)$$

Since the cross-flow velocity is far larger than the permeating flow in most cross-flow filtration, the variation of cross-flow velocity in the x-direction is neglected in this study.

(2) F_{dy}

The frictional drag in the y-direction can also be calculated by using the modified Stokes law since the Reynolds number in the filtration direction is very small in most filtration, that is

$$F_{dy} = 3\pi\mu\, d_p\, u_y\, C_y \qquad (5)$$

where u_y is the liquid velocity in the y-direction, while C_y is the correction factor due to the cake and the membrane. This correction factor can be obtained by [13]

$$C_y = 0.36\left(R_t{}'\, d_p{}^2/4\right)^{-2/5} \qquad (6)$$

where R_t' is the total filtration resistance per unit thickness of cake. Since the Reynolds number of permeating flow is very small, the variation of u_y in x-direction can be neglected, and the fully developed profile of u_y can be given by the perturbation method [8], that is,

$$u_y = q\left[1.5\left(1-\frac{y}{H}\right)-0.5\left(1-\frac{y}{H}\right)^3\right] \qquad (7)$$

where q is the filtration rate.

2. Inertial lift force

The inertial lift velocity of a particle in the flow field shown in Fig.2 can be given by [15]

$$u_l = \left(\frac{61}{576\nu}\right)\left(\frac{\tau_w}{\mu}\right)^2\left(\frac{d_p}{2}\right)^3 \qquad (8)$$

where τ_w is the shear stress acting on the membrane surface, while ν is the kinematic viscosity of liquid. Therefore, the lift force exerted on the particle can be obtained by substituting this velocity into the modified Stokes law, e.g., Eq.(5).

3. Net gravity force, F_g

The net gravity force exerted on the submerged particle can be given by

$$F_g = \frac{\pi}{6}(\rho_s-\rho)g\, d_p{}^3 \qquad (9)$$

4. Interparticle force, F_i

The DLVO theory is adopted for estimating the interparticle forces in this study. This theory claimed that there have two major long-range colloidal interactions, such as electrostatic force and van der Waals force between two approaching particles, and that the net interparticle force can be given by summing these forces [6].

5. Brownian Force, F_B

F_B is a random force due to particle collisions with the surrounding fluid molecules and can be expressed as

$$F_B = \frac{\pi}{6}\rho_s\, d_p{}^3 \cdot A(t) \qquad (10)$$

where *A(t)* is the Brownian random force exerted on per unit mass of the particle, and it follows a Gaussian distribution.

Once the forces are known, the velocities and trajectories of particles can be simulated in accordance with Eq. (1).

2.2 Deposition of particles on filter membrane

Fig.2 depicts the filtration system nearby the filter membrane, where *particle B* is a metastable particle while *particle A* is a particle just arriving at the cake surface that comes into contact with *particle B*. Each force or drag exerted on the particle has been analyzed in the previous section. The forces F_1 and F_2 are the components of the

net force whose directions are vertical and parallel to the line connecting with the gravity centers of the particles, respectively. The net forces determine whether *particle A* can deposit on the touched point or migrate to another stable position. The modes of particle migration are described as below.

1. Drag force larger than interparticle force

The drag force is dominant and exceeds the maximum repulsive force between the particles in this condition, which causes *particle A* to almost contact with *particle B.* The shortest distance between the particles is assumed to be two times the thickness of the Stern layer due to its compact matter. In such a condition, the external forces and the friction between particles are the major impact on the migration of particles. The critical angle of friction between particles can be estimated and be used to determine the stability of *particle A* [10]. If the frictional angle is smaller than its critical value, the friction between particles is large enough to cause the particle to stick stably on the contact point; otherwise, *particle A* will re-enter into the bulk flow of suspension.

2. Drag force smaller than interparticle force

If the maximum repulsive force between particles is larger than the net force of other forces in the same direction, there will exist an equilibrium distance between particles. The particles cannot actually come into contact with each other due to the repulsive force, and there is no net force acting in the direction parallel to the connecting line between the two gravity centers of the particles in equilibrium. If F_1 is not equal to zero, *particle A* will still migrate due to the lubricant effect of the double layer, and the direction of particle migration is according to the direction of F_1 . When F_1 is positive, *particle A* will leave the contact position and re-enter the bulk flow of suspension. In contrast, *particle A* will migrate into the pore of the filter cake until it deposits at another stable position or touches with more than one particle simultaneously.

3. Simulation Method

The time increment in simulation should be larger than the momentum relaxation time, $m_p/3\pi\mu d_p$ [14]; however, it must be small enough to neglect the variations of external forces in each time interval. Therefore, a time increment equal to $1x10^{-5}$ seconds is chosen in this study.

The number of particles generated within a time interval is determined by the particle balance for slurry arriving at the membrane surface, and the initial coordination of particles are determined by a numerical generator with a random distribution function. A sequence of random numbers with Gaussian distribution can be generated by the computer to estimate F_B.

According to the analyses described in the previous sections, the migration and deposition of particles can be simulated based on a periodic boundary condition. As soon as the simulation is terminated, the average porosity of the formed filter cake is estimated.

4. Analyzed System and Materials

A two-parallel-plate cross-flow microfilter with $4.5x10^{-4}$ m height, 0.1 m length, and $5.0x10^{-3}$ m width was used as the analyzed system in this study. It had a filtration area of $4.0x10^{-4}$ m^2 at the lower plate. Polymethyl methacrylate (PMMA) spherical particles with a density of 1210 kg/m^3 were used as the particulate samples. Two sizes of PMMA particles, whose mean diameters were 0.25 and 0.8 μm, respectively, were suspended in de-ionized water with a density of 1000 kg/m^3 to prepare the suspensions. The friction coefficient between particles was 0.77. The used cross-flow velocities had a range of 0.2~0.8 m/s. As a result, the Reynolds number of the suspension flow ranged from 100 to 600.

5. Results and Discussion

Fig.3 shows the packing structures of particles on the membrane surface under the same condition. The diameters of particles in Fig.3(a) are 0.25 μm; in Fig.3(b) are 0.8 μm, while in Fig.3(c) are either 0.25 or 0.8 μm in a half. It can be found that particles are packed with an angle with respect to the direction of filtration due to the tangential flow of suspension. However, this effect is not as obvious as that in cross-flow filtration of micron particles [10] because of the existence of Brownian motion of submicron particles. Comparing Figs.3(a) and (b), the packing of large particles is more compact than that of small particles due to larger normal drag exerted on large

particles. Furthermore, small particles may fill into the space among the packing of large particles when binary particles are co-existed, which results in a more compact cake.

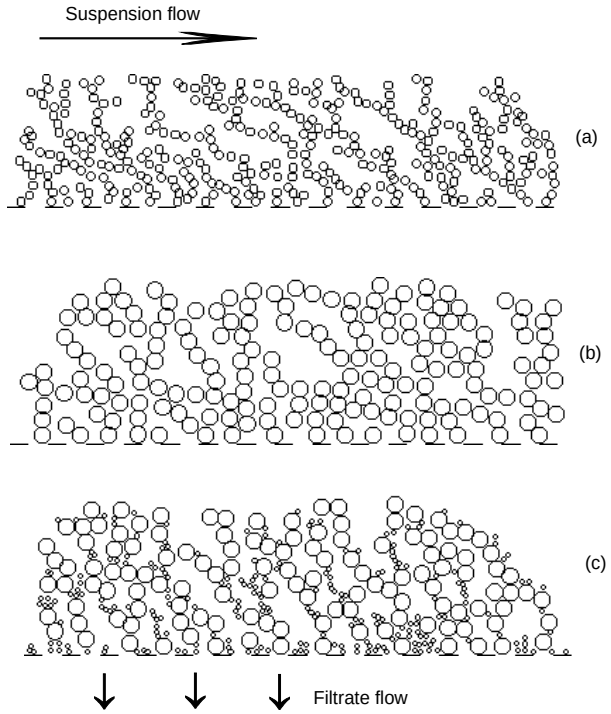

Figure 3. Packing structures of mono-sized and binary particles in cross-flow microfiltration.

Fig.4 shows the effect of cross-flow velocity on the packing structure of binary particles. The number fraction of large particles in these figures is equal to 0.5. Since the decrease of cross-flow velocity will increase the opportunities for particle deposition, a more compact cake is constructed as shown in these figures.

Another comparison of particle packing are shown in Fig.5. For a given velocity of cross-flow, an increase in filtration rate causes the stability of particles staying on the membrane surface to increase. As a result, a more compact structure will be packed under a higher filtration rate.

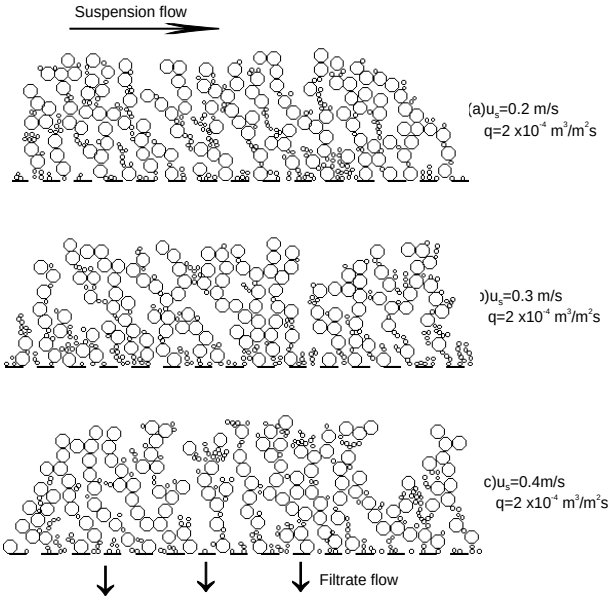

Figure 4. Packing structures of binary particles under various cross-flow velocities.

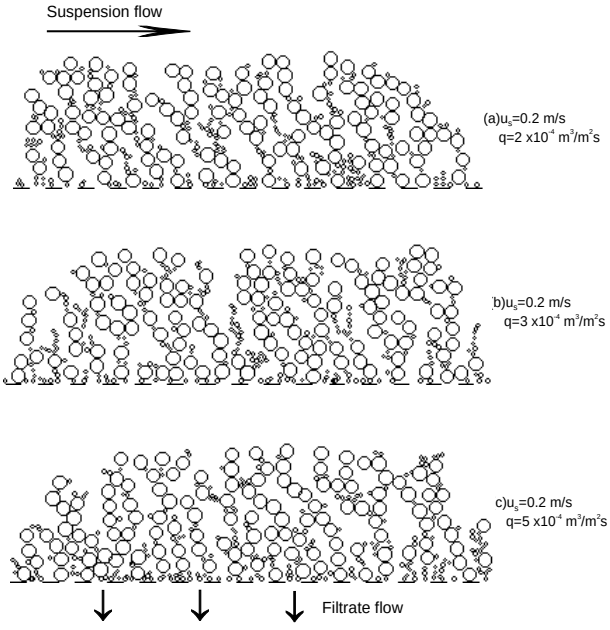

Figure 5. Packing structures of binary particles under various filtration rates.

The porosity of particle packing under various conditions are calculated and are plotted in Figs.6~7. Fig.6 illustrates how the cross-flow velocity affects the porosity of filter cake. The three regressed lines show that the packing porosity increases with the increase of cross-flow velocity of suspension. It is because the critical friction angle between particles increases with increasing cross-flow velocity. This trend is the

same as that in cross-flow filtration of micron particles [10]. Comparing with these curves, a larger filtration rate results in a lower packing porosity, and this effect is more obvious under a lower cross-flow velocity.

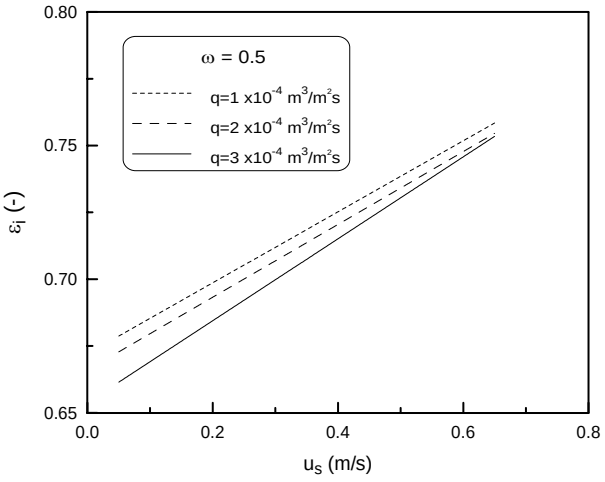

Figure 6. Effect of cross-flow velocity on the packing porosity of binary particles in cross-flow microfiltration.

Fig.7 illustrates the effect of the filtration rate on cake porosity. Since a higher filtration rate leads the depositing particles to be more easily rolling down within the filter cake, the packing porosity will decrease with the increase of filtration rate. It can be also found that the porosity increases along with the cross-flow velocity.

Fig.8 shows the effect of mixing ratio on the packing porosity of binary particles. The symbol ϕ represents the volume fraction of large particles. The simulation results have scattered values even at a given condition due to the random numbers generated by computer. The curve shown in this figure is regressed from the simulation data. It can be found that the packing porosity of mono-sized large particles is smaller than that of mono-sized small particles. It is because the drag force exerted on particles is dependent on their sized. Furthermore, when a few small particles are added into the packing of large particles ($\phi \rightarrow 1$), the packing porosity will decrease due to the cavern effect of small particles. In contrast, when large particles are added into a large amount of large particles ($\phi \rightarrow 0$), the porosity will also decrease due to the displacement effect of large particle. The lowest packing porosity is found at ϕ=0.75. Moreover, the solid triangle shown in this figure represents the experimental data for the packing of binary particles under gravity. The simulated results are higher than the experimental data for most mixing fractions due to the tangential drag exerted on particles. However, the tendencies of these data are the same, and it demonstrates the reliability of the simulation method.

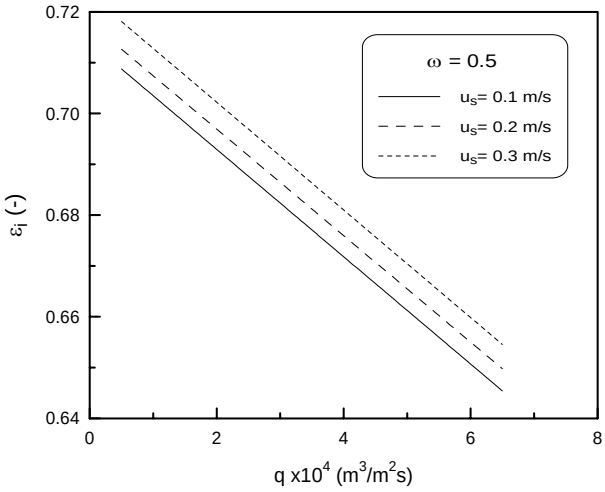

Figure 7. Effect of filtration rate on the packing porosity of binary particles in cross-flow microfiltration.

6. Conclusion

The depositions and the packing of binary submicron particles under various conditions in cross-flow microfiltration have been simulated. Based on the force analysis, the Newton's second law of motion has been integrated to calculate the velocities and displacements of particles near the membrane surface. The packing porosity of dual-sized particles was smaller than those of mono-sized. The cavern and displacement effects on the packing of binary particles have been discussed. For a given mixing fraction of particles, looser packing was constructed under a larger cross-flow velocity or under a smaller filtration rate. The impact of the mixing fraction of binary particles has been demonstrated by the experimental data of particle packing under gravity.

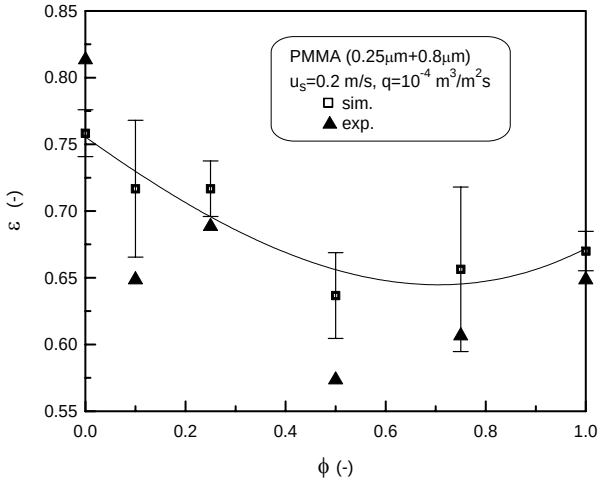

Figure 8. Comparison of simulated results and experimental data of packing porosity for various mixing fraction of binary particles in cross-flow microfiltration.

References

[1] Altena, F.W. and Belfort, G, "Lateral migration of spherical particles in porous flow channels: application to membrane filtration," *Chem. Eng. Sci*., Vol.39, No.2, pp.343-355 (1984).

[2] Ansell, G.C. and Dickinson, E., "Sediment formation by Brownian dynamic simulation: effect of colloidal and hydrodynamic interaction on the sediment structure," *J. Chem. Phys.*, Vol. 85, p.4079 (1986).

[3] Ansell, G.C. and Dickinson, E., "Brownian dynamic simulation of the fragmentation of a large colloidal floc in simple shear flow," *J. Colloid Interface Sci.*, Vol.110, p.73 (1986).

[4] Ansell, G.C. and Dickinson, E., "Short-range structure of simulated colloidal aggregates," *Phys. Rev.*, A, p.1 (1987).

[5] Fischer, E. and Raasch, J. "Cross-flow filtration," *Ger. Chem. Eng*., Vol.8, p.211 (1986).

[6] Hunter, R.J., *Foundations of Colloid Science*, Ch.7, Oxford Univ. Press, New York, (1987).

[7] Hwang, K.J., Yu, M.C., and Lu, W.M., "Migration and deposition of submicron particles in cross-flow microfiltration," Vol.32, No.17, pp.2723-2747 (1997).

[8] Ju, S.C., "A study on the mechanism of cross-flow filtration." Ph.D. Dissertation, Dept. Chem. Eng., National Taiwan University, Taiwan, R.O.C. (1988).

[9] Lu, W.M. and Ju, S.C., "Selective particle deposition in cross-flow filtration," *Sep. Sci. Technol*., Vol.24, No.7&8, p.517 (1989).

[10] Lu, W.M. and Hwang, K.J., "Cake formation in 2-D cross-flow filtration," *A.I.Ch.E. J*., Vol.41, No.6, 1443-1455 (1995).

[11] Lu, W.M., Lai, C.C., and Hwang, K.J., "Constant pressure filtration of submicron particles," *Sep. Technol.*, Vol.5, pp.45-53 (1995).

[12] O'Neill, M.E., "A sphere in contact with a plane wall in slow linear shear flow," *Chem. Eng. Sci*., Vol.23, pp.1293-1297 (1968).

[13] Sherwood, J.D., "The force on a sphere pulled away from a permeable half-space," *Physicochem. Hydrodyn.*, Vol.10, pp.3-12 (1988).

[14] Sonntag, H. and Strenge, K., *Coagulation Kinetics and Formation*, Chap.1, Uplands Press., England, (1980).

[15] Vasseur, P. and Cox, R.G., "The lateral migration of spherical particle in two dimensional shear flow," *J. Fluid Mech.*, Vol.78, p.385 (1976).

Accepted: Jun. 27, 2001